A Tin Analogue of Propadiene with Cumulated C=Sn Double Bonds

Koh Sugamata,* Teppei Asakawa, and Mao Minoura

Department of Chemistry, College of Science, Rikkyo University

sugamata@rikkyo.ac.jp

Abstract

The synthesis, structure, and properties of a stable, linear 2-stannapropadiene are reported. The identical C=Sn bonds in this 2-stannapropadiene are the shortest hitherto reported C–Sn bonds. This 2-stannapropadiene features a ^{119}Sn NMR signal at 507 ppm for the central tin atom, indicative of an unsaturated Sn^{IV} oxidation state. Treatment of this 2-stannapropadiene with $SnCl_2$·dioxane resulted in the formation of a novel four-membered cyclic 1,1-dichloro-1,3-distannetane.

Keywords

Linearly bonded tin; Heavy allenes; Single-crystal X-ray diffraction analysis; stannylene

Introduction

Zero-valent, di-coordinated group-14-element compounds, the so-called called ylidones, have been extensively studied over the last decade, and C, Si, Ge, Sn, and Pb analogues have already been reported.[1] Ylidones represent one of the isomers of the heavier analogues of allenes, albeit that most ylidones have been characterized as zero-valent compounds (E^0) rather than allenes (E^{IV}). The first 1-metallaallenes reported were the Si analogues (**A** in Figure 1) synthesized by West et al. in 1993 and the Ge analogues (**B** and **C**) independently synthesized in 1998 by West as well as Tokitoh and Okazaki.[2] Subsequently, the synthesis, reactivity, and unique properties of their analogues were investigated.[3] Interestingly, an attempted synthesis of 1-stannapropadiene (**D**) along a similar synthetic route was reported by Escudie in 2004, albeit that this led to an unprecedented stable distannirane (**E**) via a [2 + 1] cycloaddition between a transient stannylene and a 1-stannapropadiene (**D**).[4] This was the first tangible piece of evidence for the transient formation of a 1-stannapropadiene. In contrast, there is only one example each for the Si, Ge and Sn 2-metallaallene analogues (**F**, **G**, and **H**) using the same diphenythiophosphinoyl groups (Ph_2(S)P–) on the terminal carbon atoms of their allene moieties.[5] Importantly, the structural features of these compounds are not consistent with classical allene character due to the coordination of the sulfur atom in the substituents to the central metal atoms. Accordingly, tin analogues of allenes with cumulative C=Sn π-bonds have remained elusive thus far. Earlier studies have reported on the isolation and characterization of a linear 2-

germapropadiene ($\mathbf{1}_{\mathbf{Ge}}$) by using bulky silyl substituents.[6] A single-crystal X-ray electron-density-distribution (EDD) analysis of $\mathbf{1}_{\mathbf{Ge}}$ allowed us to obtain the differential electron density map of $\mathbf{1}_{\mathbf{Ge}}$, which suggested two orthogonal π-bonds for the C=Ge=C moiety. Thus, $\mathbf{1}_{\mathbf{Ge}}$ represents the first stable example of a structurally characterized germanium-centered heteroallene with a linear structure. Furthermore, the reactivity of $\mathbf{1}_{\mathbf{Ge}}$ is consistent with that of an allene rather than a tetrylone. To further investigate the properties of the corresponding 2-stannapropadiene, ^{119}Sn NMR spectroscopy should offer a useful diagnostic handle for the determination of the electronic structure of the target compound. Herein, we report the synthesis and properties of a 2-stannapropadiene ($\mathbf{1}_{\mathbf{Sn}}$). The combined results of X-ray crystallographic and NMR spectroscopic analyses suggest that $\mathbf{1}_{\mathbf{Sn}}$ exists as an allene-type structure in the solid state and in solution. The linear structure of $\mathbf{1}_{\mathbf{Sn}}$ with cumulative C=Sn double bonds was confirmed by X-ray crystallography for the first time.

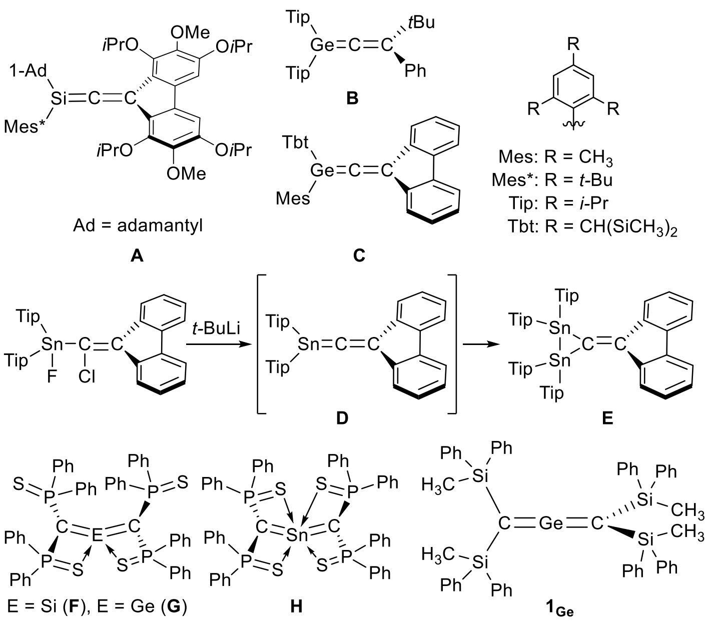

Figure 1. Heteroallenes containing heavier group-14 atoms and related compounds.

Results and discussion

As previously reported, $\mathbf{1}_{\mathbf{Ge}}$ can be obtained from the reaction between bis(silyl)carbenoid $R^{Si}{}_2CLiBr$, which is generated *in situ* from the reaction of $R^{Si}{}_2CBr_2$ with *t*-BuLi (2 eq.) in THF at –95 °C, and $GeCl_2$·dioxane (1.0 eq.) at –95 °C.[7] After removal of the generated LiBr and recrystallization from hexane and benzene, $\mathbf{1}_{\mathbf{Ge}}$ was obtained as pale-yellow crystals in 50% yield. The tin analogue ($\mathbf{1}_{\mathbf{Sn}}$) was prepared in a similar manner, *i.e.*, the bis(silyl)carbenoid was generated using the previously outlined procedure, and $SnCl_2$·dioxane (0.33 eq.) was added at low temperature (Scheme 1). After removal of all inorganic salts, recrystallization from hexane and benzene afforded 2-stannapropadiene ($\mathbf{1}_{\mathbf{Sn}}$) as yellow crystals in 57%

yield. While $\mathbf{1_{Ge}}$ formed the corresponding cyclic thermal isomer quantitatively in solution after 2 h at 60 °C upon 1,3-migration of the phenyl group, $\mathbf{1_{Sn}}$ did not undergo thermal decomposition, not even in solution after 12 h at 100 °C.

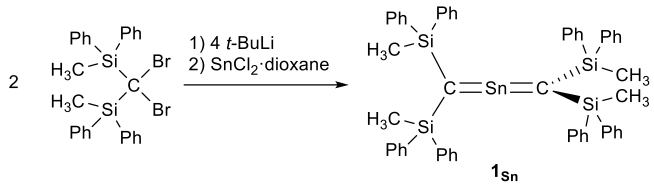

Scheme 1. Synthesis of 2-stannapropadiene $\mathbf{1_{Sn}}$.

The characterization of $\mathbf{1_{Sn}}$ was accomplished using multinuclear NMR, ultraviolet-visible (UV-vis), and infrared (IR) spectroscopy as well as mass spectrometry and single-crystal X-ray diffraction analysis (Figure 2). The solid-state structure of $\mathbf{1_{Sn}}$ exhibits D_{2d} symmetry with a linear C–Sn–C moiety (C–Sn–C angle: 178.06(6)°) and almost identical C–Sn bonds (C1–Sn1: 1.9787(15) Å; C2–Sn1: 1.9827(16) Å). These C–Sn bonds represent some of the shortest among the structurally characterized organotin species with C=Sn double bonds such as stannenes [2.003(5)–2.073(10) Å],[8] and are significantly shorter than those of a previously reported base-stabilized 2-stannapropadiene (2.063(2) Å).[5] Furthermore, the allenic moiety of the base-stabilized 2-stannapropadiene is slightly bent (171.1(1)°) with pyramidal carbon atoms (ΣC_{allene}: 354.6°). In contrast, the two terminal carbon atoms of $\mathbf{1_{Sn}}$ are almost planar (ΣC1: 359.6°; ΣC2: 359.8°), indicating that the structural properties of $\mathbf{1_{Sn}}$ are considerably different from those of the base-stabilized 2-stannapropadiene. The C1–Si1–Si2 and C2–Si3–Si4 planes slightly deviate from a perpendicular arrangement relative to each other (79.9°), probably due to the steric repulsion among the silyl groups.

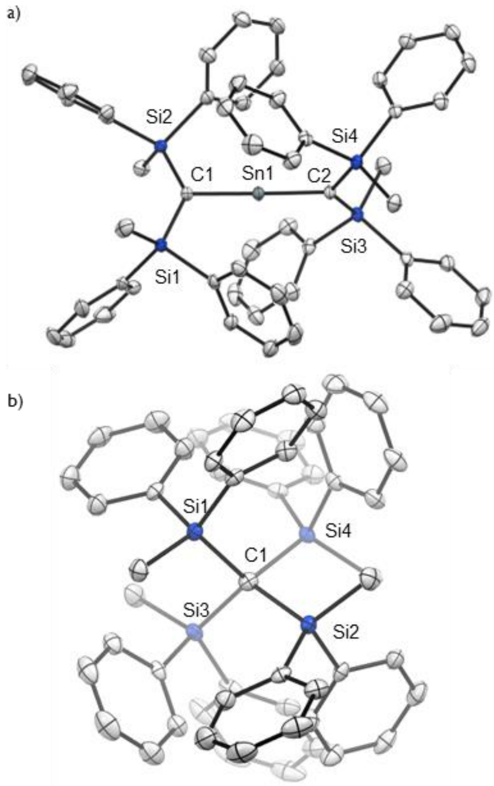

Figure 2. a) Top and b) side view of the molecular structure of $\mathbf{1_{Sn}}$ with thermal ellipsoids at 50% probability; hydrogen atoms are omitted for clarity. Selected bond lengths [Å] and angles [°] for $\mathbf{1_{Sn}}$: C1–Sn1: 1.9787(15), C2–Sn1: 1.9827(16), C1–Si1: 1.8410(16), C1–Si2: 1.8336(16), C2–Si3: 1.8423(16), C2–Si4: 1.8428(16), C1−Sn−C2: 178.06(6), Si1−C1−Si2: 130.90(9), Si1−C1−Sn1: 114.62(8), Si2−C1−Sn1: 114.07(8), Si3−C2−Si4: 133.33(9), Si3−C2−Sn1: 112.17(8), Si4−C2−Sn1: 114.29(8).

The molecular structure of $\mathbf{1_{Sn}}$ was further examined using theoretical calculations. The structural characteristics of $\mathbf{1_{Sn}}$, which were optimized at the B3PW91-D3(bj)/def2TZVP level for Sn and the 6-311G(2d,p) level for the rest of the atoms, are in good agreement with those obtained experimentally (Figure S27), *i.e.*, the linear geometry of the C=Sn=C moiety (C–Sn–C = 180.0°) and the two C–Sn bond lengths (1.959 Å) are close to the values obtained from the XRD analysis (C1–Sn1: 1.9787(15) Å; C2–Sn1: 1.9827(16) Å). The introduction of H_3Si substituents on the 2-stannapropadiene ($\mathbf{1_{Sn}^{H3Si}}$) resulted in an optimized linear structure, whereas the H-, H_3C-, and H_2N-substituted 2-stannapropadienes $\mathbf{1_{Sn}^{H}}$, $\mathbf{1_{Sn}^{H3C}}$, and $\mathbf{1_{Sn}^{H2N}}$ exhibit bent structures, suggesting that the presence of silyl substituents on the terminal carbon atoms can be expected to affect the linear C=Sn=C structure of $\mathbf{1_{Sn}}$. The C–Sn–C angle decreases with increasing electron-donating properties of the substituents on the terminal carbons ($\mathbf{1_{Sn}^{H2N}}$: 91.1°; $\mathbf{1_{Sn}^{H3C}}$: 100.2°; $\mathbf{1_{Sn}^{H}}$: 150.4°; $\mathbf{1_{Sn}^{H3Si}}$: 180.0°). The frontier Kohn–Sham orbitals of $\mathbf{1_{Sn}}$ provide further information on the nature of the cumulated C=Sn bonds. The HOMO (π), HOMO−1 (π), LUMO (π*), and LUMO+1 (π*) of $\mathbf{1_{Sn}}$ revealed features typical of compounds with a linear allene-type structure (Figure 3b). A natural bond orbital (NBO) analysis of the optimized structure of **1**$_{Sn}$ showed two C–Sn π-bonds consisting of almost pure 5p orbitals of the tin atom and 2p orbitals of the carbon atoms on the allene moiety.[9] The calculated natural-population-analysis (NPA) charge on the tin atom was +2.06, while the charge on each of the terminal carbon atoms was –1.95, which indicates a stronger polarization in the allene moiety of **1**$_{Sn}$ compared to that of the germanium derivative **1**$_{Ge}$ (Ge: +1.76; C: –1.86).[6]

To investigate the multiple-bond character of **1**$_{Sn}$ by vibrational spectroscopy, we recorded the IR spectrum (KBr, pellet) of **1**$_{Sn}$ in the solid state (Figure S34). The C=Sn=C asymmetric stretching frequency of **1**$_{Sn}$ was observed at 930 cm^{-1} and the assignment of this IR shift was supported by DFT calculations (925 cm^{-1}). This frequency is slightly lower than the C=Ge=C asymmetric stretching frequency of **1**$_{Ge}$ (973 cm^{-1}) and significantly lower than the C=C=C asymmetric stretching frequency of 1,1,3,3-tetrakis(trimethylsilyl)allene (1870 cm^{-1}).[10] It can thus be concluded that the frequency of the stretching vibration reflects the bond strength of the allene moieties.

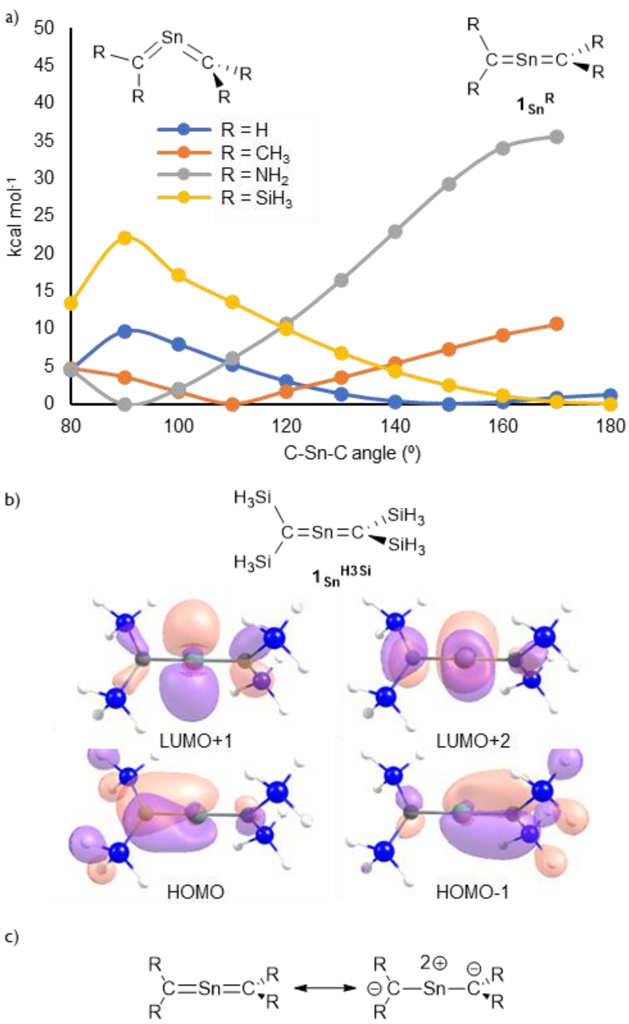

Figure 3. a) Optimized structures of 2-stannapropadienes calculated at the B3PW91-D3(bj)/Def2TZVP level for Sn and the 6-311G(2d,p) level for the rest of the atoms. b) Kohn–Sham orbitals of **1**$_{Sn}^{H3Si}$. c)

Canonical resonance structures of linear 2-stannapropadienes.

In the ^{1}H NMR spectrum of **1$_{Sn}$** in C_6D_6, the signal for the protons of the methyl groups was observed as a sharp singlet at 0.39 ppm, indicating a highly symmetric structure for **1$_{Sn}$** in solution. The resonance for the carbon nuclei of the terminal carbons in the allene moiety was observed at 107 ppm, which is shifted slightly down-field relative to those of previously reported 2-germapropadiene **1$_{Ge}$** (86 ppm) and tetrakis(trimethylsilyl)allene (64 ppm).[9] Moreover, the ^{119}Sn NMR signal for the tin atom was observed at 507 ppm in C_6D_6, indicating unsaturated Sn^{IV} character, similar to those of stable stannenes (270–835 ppm) and the stannaaromatic compounds (264–491 ppm) shown in Figure 4.[11] However, this value is significantly lower than those of reported stannylones ((-1147)–64 ppm), which are zero-valent tin species, and higher than those of kinetically stabilized stannylenes (2235–2323 ppm), which are Sn^{II} species.[12] The central tin atom of a tristannaallene has been observed at 2233 ppm due to the considerable unsaturated character that is similar to that in stannylenes, and a stereochemically active lone pair of electrons.[13] In contrast to the resonance of the ^{119}Sn nucleus in the base-stabilized 2-stannapropadiene (-401 ppm), the resonance of **1$_{Sn}$** is characteristic for an unsaturated tin compound.[5] Moreover, the ^{119}Sn NMR signal of **1$_{Sn}$** in THF at 20 °C was observed as a broadened peak at 497 ppm. The signal showed a gradual shift to higher field with decreasing temperature (Figure S22), suggesting a dynamic process. At –50 °C, the signals were observed at 475 ppm and 362 ppm. Gauge-independent atomic orbital (GIAO) ^{119}Sn NMR calculations for the optimized structure of **1$_{Sn}$** afforded a value of 849 ppm. When the solvent effect for THF was considered using the SCRF method, no significant shift in the signal was observed (847 ppm). However, for **1$_{Sn}$·THF**, wherein one molecule of THF is coordinated to the central tin atom, a significant signal shift to 539 ppm was observed. The optimized structure of **1$_{Sn}$·THF** revealed a bent C–Sn–C moiety (Figure S28), and this distortion in the molecular geometry around the tin atom could feasibly account for the observed changes of the chemical shifts. To investigate the dynamics of **1$_{Sn}$** in THF, variable-temperature ^{1}H NMR experiments were carried out. As shown in Figure S21, the methyl protons of **1$_{Sn}$** were observed as a broadened peak at 0.20 ppm at room temperature. At –50 °C, these protons were observed as two independent sharp singlet signals (0.31/0.16) with 1:3 ratio. However, at 40 °C, all methyl protons appear as a sharp singlet, suggesting rapid dissociation of the coordinated THF molecule from the central tin atom of **1$_{Sn}$**.

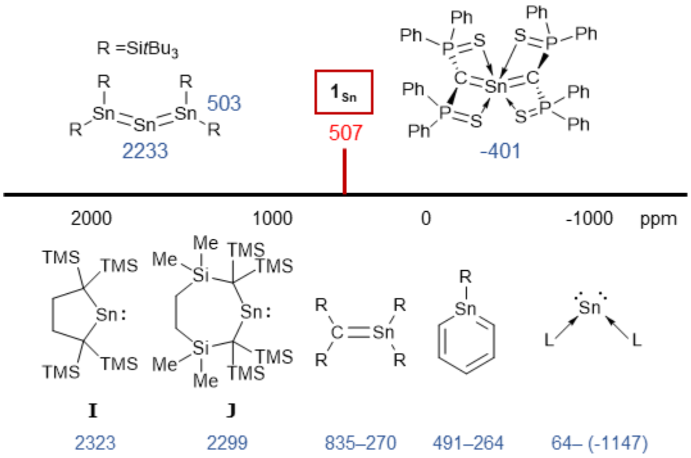

Figure 4. [119]Sn NMR chemical shifts of $\mathbf{1}_{\mathbf{Sn}}$ and related compounds.

The ultraviolet-visible (UV-vis) spectrum of $\mathbf{1}_{\mathbf{Sn}}$ in benzene shows an absorption maximum at λ_{max} = 328 nm (ε 8000 dm^3 mol^{-1} cm^{-1}), indicating isolated π-bonding without any conjugation (Figure 5). This value is red-shifted relative to those of $\mathbf{1}_{\mathbf{Ge}}$ [265 nm (ε 11000 dm^3 mol^{-1} cm^{-1}), 272 nm (ε 12000 dm^3 mol^{-1} cm^{-1}), and 283 nm (ε 11000 dm^3 mol^{-1} cm^{-1})] and tetrakis(trimethylsilyl)allene[10] (273 nm, ε 36000 dm^3 mol^{-1} cm^{-1}), indicating a narrowing of the HOMO–LUMO gap of $\mathbf{1}_{\mathbf{Sn}}$ relative to that of the germanium analogue $\mathbf{1}_{\mathbf{Ge}}$ due to the insufficient orbital overlap of 5pπ–2pπ in $\mathbf{1}_{\mathbf{Sn}}$ relative to 4pπ–2pπ in $\mathbf{1}_{\mathbf{Ge}}$ (Figure S32). The UV-vis spectrum of $\mathbf{1}_{\mathbf{Sn}}$ in THF at room temperature exhibits a pronounced shoulder peak at 430 nm, which can be attributed to the coordination of a THF molecule to the central tin atom of $\mathbf{1}_{\mathbf{Sn}}$ (Figure S37). However, at 50 °C, the shoulder peak at 430 nm disappeared due to the dissociation of the coordinated THF molecule. Similarly, when donor molecules such as pyridine and 4-dimethylaminopyridine (DMAP) were added to a benzene solution of $\mathbf{1}_{\mathbf{Sn}}$, similar shoulder peaks were observed in the respective spectra (Figure S36). Time-dependent density functional theory (TD-DFT) calculations were performed for compounds $\mathbf{1}_{\mathbf{Sn}}$ and **$\mathbf{1}_{\mathbf{Sn}}$·donor** at the B3PW91/def2tzvp level for Sn and the 6-311++g(2d,p) level for all other atoms. The results indicate a mixture of two π–π* transitions, *i.e.*, one at 333 nm (f = 0.0178) and another at 306 nm (f = 0.1589), which are in good agreement with the observed λ_{max} value for $\mathbf{1}_{\mathbf{Sn}}$. For **$\mathbf{1}_{\mathbf{Sn}}$·THF**, the calculations suggest a mixture of two π–π* transitions associated with the bent allene moiety, whereby one occurs at 443 nm (f = 0.0067), consistent with the experimentally observed λ_{max} value. According to the theoretical calculations, the coordination of the donor molecule to $\mathbf{1}_{\mathbf{Sn}}$ to form **$\mathbf{1}_{\mathbf{Sn}}$·donor** (donor: THF, pyridine, or DMAP) is expected to be exothermic for all cases except for THF (for details, see Table S34). While the coordination of the donor molecule THF to the central tin atom of $\mathbf{1}_{\mathbf{Sn}}$ is endothermic, it is still likely that THF coordinates to the central tin atom in solution. The coordinated molecules of THF readily dissociate upon solvent distillation to regenerate $\mathbf{1}_{\mathbf{Sn}}$. Recrystallization in the presence of THF or DMAP leads to the formation of $\mathbf{1}_{\mathbf{Sn}}$, indicating that the coordination of these donors to $\mathbf{1}_{\mathbf{Sn}}$ in the crystalline solid state is not favorable. The higher positive charge on the central tin atom in $\mathbf{1}_{\mathbf{Sn}}$, coupled with its lower steric demand compared to that of germanium derivative ($\mathbf{1_{Ge}}$), suggests a preference for the coordination of donor molecules to the central tin atoms.

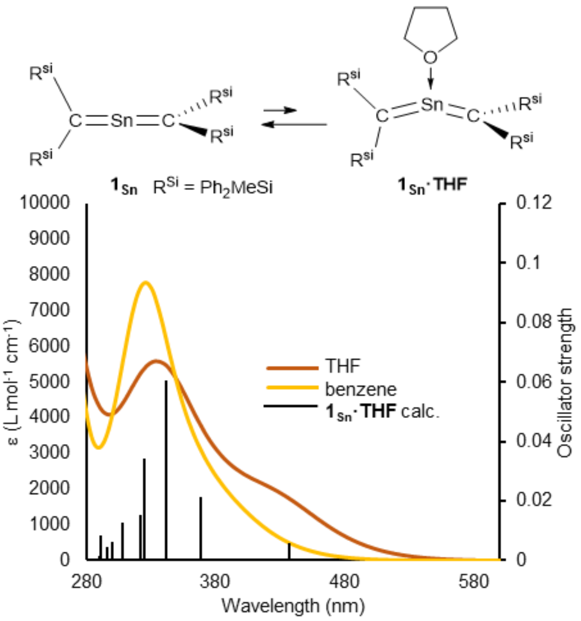

Figure 5. a) UV-vis spectra of $\mathbf{1_{Sn}}$ in benzene and THF at room temperature, and simulated UV-vis absorption spectrum of $\mathbf{1_{Sn}}$·**THF** obtained from TD-DFT calculations, together with theoretical oscillator-strength values (black vertical lines).

The reaction of $\mathbf{1_{Sn}}$ with H_2O immediately produced stannanediol **2** (Scheme 2). Subsequently, the reaction of $\mathbf{1_{Sn}}$ with 2 eq. of MeLi followed by H_2O afforded the corresponding demethylated compound **3**. As expected, $\mathbf{1_{Sn}}$ readily reacts with hydrogen chloride under mild conditions to quantitatively form the corresponding dichlorostannane (**4**). These reactivity patterns are similar to those of 2-germapropadiene ($\mathbf{1_{Ge}}$), indicating that the central tin atom can be expected to be the most electrophilic atom in the C=Sn=C allene moiety. In order to further explore the reactivity of $\mathbf{1_{Sn}}$, we undertook an investigation involving the reaction between $\mathbf{1_{Sn}}$ and the $SnCl_2$·dioxane complex. This reaction was motivated by our previous syntheses of four-membered cyclic compounds derived from bis(methylene)-λ^4-chalcogenanes using GeX_2·dioxane (X = Cl, Br).[13] The reaction of $\mathbf{1_{Sn}}$ with $SnCl_2$·dioxane proceeded smoothly even at room temperature to afford the corresponding four-membered stannylene **5** as orange crystals, which are thermally stable but sensitive to H_2O, which affords decomposed **4** selectively.

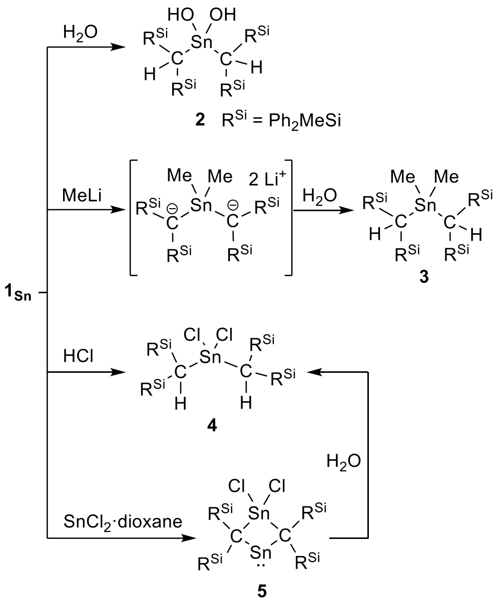

Scheme 2. Reactivity patterns of **1$_{Sn}$**.

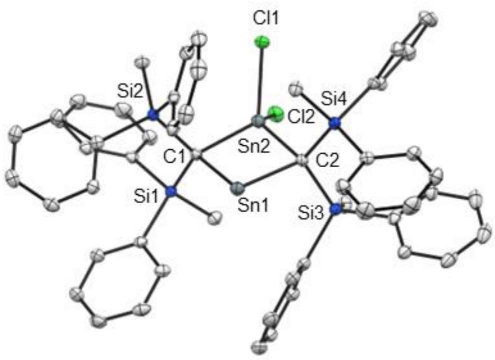

Figure 6. Molecular structure of **5** with thermal ellipsoids at 50% probability; hydrogen atoms are omitted for clarity. Selected bond lengths [Å] and angles [°] for **1$_{Sn}$**: C1–Sn1: 2.313(2), C2–Sn1: 2.301(2), C1–Sn2: 2.163(2), C2–Sn2: 2.173(2), C1–Si1: 1.905(2), C1–Si2: 1.888(2), C2–Si3: 1.902(2), C2–Si4: 1.909(2), C1−Sn1−C2: 87.93(8), C1–Sn2–C2: 95.22(8), Sn1–C1–Sn2: 87.67(8), Sn1–C2–Sn2: 78.76(8).

The experimental molecular structure and theoretical calculations suggest that **5** contains a Sn^{II} and a Sn^{IV} atom (Figure 6). The shortest distance between divalent tin atoms in **5** is 7.20 Å, which indicates that **5** is monomeric in the solid state. In contrast, there is a weak intermolecular interaction between Sn1···Sn2 in **5** (3.1022(5) Å), which is shorter than the sum of the van der Waals radii (4.34 Å).[15] The Sn1 center adopts a typical di-coordinated Sn^{II} geometry, and the Sn2 center shows a typical tetra-coordinated Sn^{IV} geometry. The C1–Sn1–C2 bond angle of **5** (87.93(5)°) is similar to that of a previously reported five-membered dialkylstannylene (86.7(2)°).[12a] The Sn1–C bond lengths in **5** (2.313(2) Å and 2.300(2) Å) are significantly longer than those of a hitherto reported dialkylstannylene (2.218(7) Å and 2.223(7) Å), indicating slight amounts of strain due to the four-membered ring in **5**. The bond length of Sn2–C (2.163(2) Å and 2.173(2) Å) is almost identical to that of typical Sn–C bonds (2.16 Å), indicating an increased p-character of the central Sn^{II} atom in the Sn1–C single bonds in **5** relative to that in $\mathbf{1_{Sn}}$. The four-membered ring of **5** deviates slightly from planarity (sum of the interior angles: 358.58°). In the ^{1}H, ^{13}C, and ^{29}Si NMR spectra of **5** in C_6D_6 at room temperature, a signal for only one set of silyl groups was observed, suggesting a flipping of the four-membered ring of **5**. The ^{119}Sn NMR spectrum of **5** in C_6D_6 exhibits signals at 1355 ppm for the Sn^{II} nucleus and at 61 ppm for the Sn^{IV} nucleus. The signal for the Sn^{II} nucleus of **5** is shifted upfield relative to those of the kinetically stabilized stannylenes (**I**: 2323 ppm; **J**: 2299 ppm; Figure 4),[12] indicating some manner of interactions with the Sn^{II} nucleus. To investigate the interactions with Sn^{II}, NBO calculations were conducted at the B3PW91-D3(bj)/def2tzvp level for Sn and the 6-311+G(2d,p) level for the rest of the atoms. The vacant p orbital of Sn^{II} in **5** receives electron donation from not only the C–Si σ-bonds but also the C–Sn^{IV} bonds and p orbitals of the phenyl groups. This would increase the electron density on Sn^{II}, resulting in a significant upfield shift of the ^{119}Sn signal of **5**. In Figure S38, the UV-vis spectrum of **5** in benzene shows an absorption maximum at λ_{max} = 466 nm (ε 1260 dm^3 mol^{-1} cm^{-1}), which is slightly blue-shifted compared to that of the five-membered cyclic stannylene **I** (484 nm; ε 400 dm^3 mol^{-1} cm^{-1}) in Figure 4. Moreover, the absorption coefficients of **5** are significantly higher than that of **I**, suggesting an expansion between the phenyl moieties and the vacant p orbital of Sn^{II} observed using DFT calculations for **5**. Further studies of the reactivity of **5** are currently in progress.

Conclusion

In conclusion, we have reported the successful synthesis of the first stable 2-stannapropadiene ($\mathbf{1_{Sn}}$) with a linear allene-type structure. The bulky silyl groups dominate the structural features and govern the stability of the 2-stannapropadiene due to the high steric demand and negative hyperconjugation by the silyl groups. A multinuclear NMR analysis of the linear heteroallene confirmed the unsaturated Sn^{IV} oxidation state of the central Sn atom. The reaction of $\mathbf{1_{Sn}}$ with $SnCl_2$·dioxane afforded the corresponding four-membered cyclic stannylene (**5**), indicating a unique reactivity unlike that of a previously reported 2-germapropadiene. Further investigations into the reactivity of $\mathbf{1_{Sn}}$ and **5**, including the reduction of four-membered cyclic stannylene (**5**), are currently in progress in our laboratories.

Funding Sources
This research was funded by JSPS KAKENHI grants JP18K14204 and 20K05468 from MEXT (Japan).

Supporting Information

Experimental procedures, NMR data, X-ray crystallographic analysis, computational details, IR spectroscopic analysis, and UV-vis spectroscopic analysis (PDF). Computational data of coordinates (xyz).

Accession Codes

CCDC 2288705-2288708 contain the supplementary crystallographic data for this paper. These data can be obtained free of charge via www.ccdc.cam.ac.uk/data_request/cif, by emailing data_request@ccdc.cam.ac.uk, or by contacting the Cambridge Crystallographic Data Centre, 12 Union Road, Cambridge CB2 1EZ, UK; fax: +44 1223 336033.

Acknowledgements

We would like to thank Dr. Nobuhiro Yasuda, Dr. Kunihisa Sugimoto, and Dr. Yuiga Nakamura at JASRI BL02B1 of SPring-8, where X-ray diffraction data were collected under project numbers 2021A1592, 2021A1578, 2021B1435, 2021B1833, 2021B1132, 2021B1798, 2022A1200, 2022A1584, 2022B1626, 2023A1727, 2023A1771, and 2023A1925.

References

1. a) M. Wu, Y. He, L. Zhang, R. Wei, D. Wang, J. Liu, L. L. Liu, G. Tan, *Eur. J. Inorg. Chem.* **2022**, *31,* e202200413. b) T. Koike, T. Nukazawa, T. Iwamoto, *J. Am. Chem. Soc.* **2021**, *143*, 14332–14341. c) S. Yao, A. Kostenko, Y. Xiong, A. Ruzicka, M. Driess, *J. Am. Chem. Soc.* **2020**, *142*, 12608–12612. d) Y. Wang, M. Karni, S. Yao, A. Kaushansky, Y. Apeloig, M. Driess, *J. Am. Chem. Soc.* **2019**, *141*, 12916–12927. e) T. Sugahara, T. Sasamori, N. Tokitoh, *Angew. Chem., Int. Ed.* **2017**, *56*, 9920–9923. F) Y. Xiong, S. Yao, S. Inoue, J. D. Epping, M. Driess, *Angew. Chem., Int. Ed.* **2013**, *52*, 7147–7150. g) K. C. Mondal, H. W. Roesky, M. C. Schwarzer, G. Frenking, B. Niepötter, H. Wolf, R. Herbst-Irmer, D. Stalke, *Angew. Chem., Int. Ed.* **2013**, *52*, 2963–2967. h) P. K. Majhi, T. Sasamori, *Chem.-Eur. J.* **2018**, *24*, 9441–9455. i) J. Xu, C. Dai, S. Yao, J. Zhu, M. Driess, *Angew. Chem., Int. Ed.* **2022**, *61*, e202114073. j) J. Xu, S. Pan, S. Yao, G. Frenking, M. Driess, *Angew. Chem., Int. Ed.* **2022**, *61*, e202209442.
2. a) G. E. Miracle, J. L. Ball, D. R. Powell, R. West, *J. Am. Chem. Soc.* **1993**, *115*, 11598–11599. B) B. E. Eichler, D. R. Powell, R. West, *Organometallics* **1998**, *17*, 2147–2148. C) N. Tokitoh, K. Kishikawa, R. Okazaki, *Chem. Lett.* **1998**, *27*, 811–812.
3. a) B. Eichler, R. West, in *Advances in Organometallic Chemistry*, Academic Press, **2000**, pp. 1–46. B) B. E. Eichler, G. E. Miracle, D. R. Powell, R. West, *Main Group Met. Chem.* **1999**, *22*, 147–162. C) B. E. Eichler, D. R. Powell, R. West, *Organometallics* **1999**, *18*, 540–545. D) M. Trommer, G. E. Miracle, B. E. Eichler, D. R. Powell, R. West, *Organometallics* **1997**, *16*, 5737–5747.
4. L. Baiget, H. Ranaivonjatovo, J. Escudié, H. Gornitzka, *J. Am. Chem. Soc.* **2004**, *126*, 11792–11793.
5. a) C. Foo, K.-C. Lau, Y.-F. Yang, C.-W. So, *Chem. Commun.* **2009**, 6816–6818. B) W.-P. Leung, Y.-C.

Chan, T. C. W. Mak, *Inorg. Chem.* **2011**, *50*, 10517–10518. C) Y.-F. Yang, C. Foo, H.-W. Xi, Y. Li, K. H. Lim, C.-W. So, *Organometallics* **2013**, *32*, 2267–2270.

6. K. Sugamata, T. Asakawa, D. Hashizume, M. Minoura, *Angew. Chem., Int. Ed.* **2023**, *62*, e202302836.
7. A. Inoue, J. Kondo, H. Shinokubo, K. Oshima, *Chem. Lett.* **2001**, *30*, 956–957.
8. a) R. C. Fischer, P. P. Power, *Chem. Rev.* **2010**, *110*, 3877–3923. b) H. Meyer, G. Baum, W. Massa, S. Berger, A. Berndt, *Angew. Chem., Int. Ed Engl.* **1987**, *26*, 546–548. c) G. Anselme, H. Ranaivonjatovo, J. Escudie, C. Couret, J. Satge, *Organometallics* **1992**, *11*, 2748–2750. d) Y. Mizuhata, N. Takeda, T. Sasamori, N. Tokitoh, *Chem. Commun.* **2005**, 5876–5878. e) A. Fatah, R. El Ayoubi, H. Gornitzka, H. Ranaivonjatovo, J. Escudié, *Eur. J. Inorg. Chem.* **2008**, *2008*, 2007–2013.
9. Natural-bond-orbital (NBO) analysis of $\mathbf{1}_{\mathbf{Sn}}$: a) C1-Sn: 1.973 e, C1 (64.90%, sp4.34) + Sn (35.10%, sp0.07), b) C1-Sn: 1.877 e, C1 (84.40%, p) + Sn (15.60%, p), c) C2-Sn: 1.877 e, C2 (84.40%, p) + Sn (15.60%, p), d) C2: 1.422 e, C2 (sp3.70) f) Sn: 0.259 e, Sn(sp14.17); E. D. Glendening, C. R. Landis, F. Weinhold, *J. Comput. Chem.* **2019**, *40*, 2234–2241.
10. a) R. West, P. C. Jones, *J. Am. Chem. Soc.* **1969**, *91*, 6156–6161. b) A. de Meijere, D. Faber, U. Heinecke, R. Walsh, T. Müller, Y. Apeloig, *Eur. J. Org. Chem.* **2001**, *2001*, 663–680.
11. a) C. Kaiya, K. Suzuki, M. Yamashita, *Angew. Chem., Int. Ed.* **2019**, *58*, 7749–7752. b) Y. Mizuhata, N. Noda, N. Tokitoh, *Organometallics* **2010**, *29*, 4781–4784. c) Y. Mizuhata, T. Sasamori, N. Takeda, N. Tokitoh, *J. Am. Chem. Soc.* **2006**, *128*, 1050–1051. d) Y. Mizuhata, N. Takeda, T. Sasamori, N. Tokitoh, *Chem. Lett.* **2005**, *34*, 1088–1089.
12. a) M. Kira, R. Yauchibara, R. Hirano, C. Kabuto, H. Sakurai, *J. Am. Chem. Soc.* **1991**, *113*, 7785–7787. b) C. Eaborn, M. S. Hill, P. B. Hitchcock, D. Patel, J. D. Smith, S. Zhang, *Organometallics* **2000**, *19*, 49–53.
13. N. Wiberg, H.-W. Lerner, S.-K. Vasisht, S. Wagner, K. Karaghiosoff, H. Nöth, W. Ponikwar, *Eur. J. Inorg. Chem.* **1999**, *1999*, 1211–1218.
14. a) K. Sugamata, T. Asakawa, Y. Urao, M. Minoura, *Inorg. Chem.* **2022**, *61*, 17641–17645. b) K. Sugamata, Y. Urao, M. Minoura, *Chem. Commun.* **2019**, *55*, 8254–8257. c) K. Sugamata, D. Hashizume, Y. Suzuki, T. Sasamori, S. Ishii, *Chem.-Eur. J.* **2018**, *24*, 6922–6926.
15. M. Mantina, A. C. Chamberlin, R. Valero, C. J. Cramer, D. G. Truhlar, *J. Phys. Chem. A* **2009**, *113*, 5806–5812.